Plasmonic Nanocatalysts

DOI: 10.1002/ange.201309759

Surfactant-Free Nonaqueous Synthesis of Plasmonic Molybdenum Oxide Nanosheets with Enhanced Catalytic Activity for Hydrogen Generation from Ammonia Borane under Visible Light**

*Hefeng Cheng, Takashi Kamegawa, Kohsuke Mori, and Hiromi Yamashita**

Abstract: *Plasmonic materials have drawn emerging interest, especially in nontraditional semiconductor nanostructures with earth-abundant elements and low resistive loss. However, the actualization of highly efficient catalysis in plasmonic semiconductor nanostructures is still a challenge, owing to the presence of surface-capping agents in their synthetic procedures. To fulfill this, a facile non-aqueous procedure was employed to prepare well-defined molybdenum oxide nanosheets in the absence of surfactants. The obtained MoO_{3-x} nanosheets display intense absorption in a wide range attributed to the localized surface plasmon resonances, which can be tuned from the visible to the near-infrared region. Herein, we demonstrate that such plasmonic semiconductor nanostructures could be used as highly efficient catalysts that dramatically enhance the hydrogen-generation activity of ammonia borane under visible light irradiation.*

Arising from resonant excitation, collective oscillations of free carriers in nanostructured materials could strongly concentrate and amplify the incident light intensity in the vicinity of their surface. Such a near-field enhancement phenomenon, which is known as localized surface plasmon resonance (LSPR), is capable of harvesting light at the nanoscale, and has found promising applications in diverse areas, such as single-molecule spectroscopy, photothermal therapy, catalysis, and photovoltaics.[1–3] As the most common plasmonic materials, noble metals such as Au and Ag usually possess high carrier density (10^{22}–10^{23} cm^{-3}) and display apparent LSPR over a wide range from the ultraviolet (UV) region to the near infrared (NIR).[4] Moreover, their plasmonic frequencies are highly dependent on their sizes and shapes, as well as the surrounding mediums.[5] Despite the easy manipulation of LSPR, noble metals inevitably suffer from earth rarity and high resistive loss,[6] which prevent them from being used in large scale practical applications.

Recently, it has been revealed that LSPR can also occur in some heavily doped semiconductor nanocrystals with an appreciable free carrier concentration, including indium tin oxides (ITO),[7] copper chalcogenides,[8] and transition-metal oxides.[9–12] For example, WO_{3-x} nanorods have been prepared and showed strong NIR absorption with an LSPR peak at approximately 900 nm.[10] With respect to noble metals, the plasmonic resonance of semiconductors could be tailored by changing the stoichiometric compositions, dopant concentrations, or phase transitions.[13] In most cases, syntheses of plasmonic semiconductor nanostructures are resorted to the conventional "hot injection" routes, in which surfactants (e.g., oleylamine and trioctylphosphine oxide) allow precise control over the size and monodispersity. However, the use of surface-capping agents generally leads to unpredictable cytotoxic effects. It also lowers the surface feasibility of nanocrystals for use in the fields of sensing and catalysis. Therefore, it is of crucial importance to develop rational surfactant-free approaches to plasmonic semiconductor nanostructures, which could provide the versatile synthetic alternative and optimize their catalytic performances.

Herein, we illustrate a facile nonaqueous access to MoO_{3-x} nanosheets without the addition of any surfactants, which showed strong LSPR in the visible light region. Experimental parameters, such as synthetic temperatures and reacting solvents, were found to play important roles in the phase and morphology evolution of molybdenum oxide nanostructures, accompanied by the tunable LSPR from the visible region to the NIR. We further demonstrated that, under visible light irradiation ($\lambda > 420$ nm), such plasmonic MoO_{3-x} nanosheets displayed dramatically enhanced molecular hydrogen production from ammonia borane (NH_3BH_3), which may open up the new prospective possibility of the plasmonic semiconductor nanostructures for highly efficient heterogeneous catalysis.

MoO_{3-x} nanosheets were prepared by oxidizing metal molybdenum powders with hydrogen peroxide (H_2O_2, 30%) followed by solvothermal treatment in ethanol solution at 160 °C for 12 h (see the Supporting Information for details). The collected products exhibit intense blue color, as shown in Figure 1a. Such blue molybdenum oxide species (denoted as MoO_{3-x}) were quite stable in air and could maintain their original color for several months. It has been well documented that the blue color of transition oxides originates from the characteristic outer d-shell electrons, as is the case with deficient WO_{3-x}[10] and TiO_{2-x}.[11] Besides, the blue MoO_{3-x} sample turned white after annealing at 300 °C in air, further confirming the presence of oxygen vacancies.

[*] H. Cheng, Dr. T. Kamegawa, Dr. K. Mori, Prof. Dr. H. Yamashita
Graduate School of Engineering, Osaka University
2-1 Yamada-oka, Suita, Osaka 565-0871 (Japan)
E-mail: yamashita@mat.eng.osaka-u.ac.jp
Dr. T. Kamegawa, Dr. K. Mori, Prof. Dr. H. Yamashita
Unit of Elements Strategy Initiative for Catalysts & Batteries, ESICB, Kyoto University (Japan)

[**] The X-ray absorption measurements were performed at SPring-8, Harima (Japan). H.C. acknowledges the Japan Society for the Promotion of Science (JSPS) for the fellowship.

Supporting information for this article is available on the WWW under http://dx.doi.org/10.1002/anie.201309759.

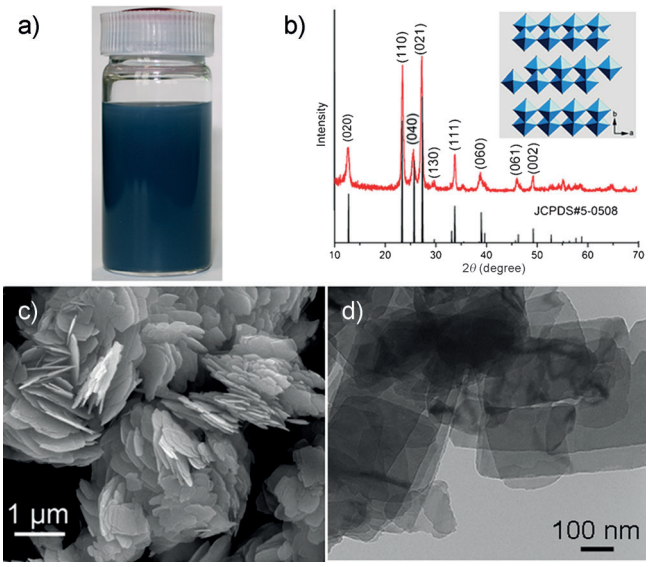

Figure 1. a) A photograph of the MoO_{3-x} product dispersed in ethanol. b) XRD pattern of MoO_{3-x} and (inset) crystal structure of the orthorhombic MoO_3. SEM (c) and TEM (d) images of the MoO_{3-x} products.

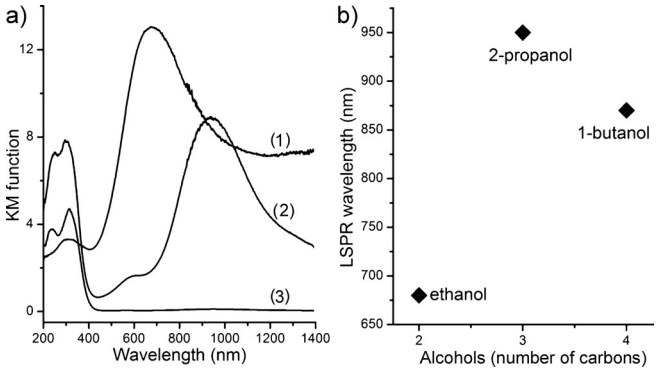

Figure 2. a) UV/Vis–NIR diffuse reflectance spectra of the MoO_{3-x} samples prepared at 160 °C (1) and 140 °C (2) for 12 h, and commercial MoO_3 (3). b) The LSPR wavelength of the products prepared by different alcohols in the solvothermal synthesis.

From the X-ray diffraction pattern (XRD; Figure 1 b), the product is assigned to the orthorhombic phase (JCPDS No. 5-0508), which is crystallized in a layered structure composed of MoO_6 octahedra by sharing edges and corners (inset). Figure 1 c presents the typical scanning electron microscopy (SEM) image of the as-prepared MoO_{3-x} products, from which numerous two-dimensional (2D) nanosheets were observed. The diameter of the MoO_{3-x} nanosheets ranges from 200 nm to 1 μm, and the thickness is about 20–30 nm. Transmission electron microscopy image (TEM; Figure 1 d) further confirms the products in the shape of nanosheets. The formation of 2D MoO_{3-x} nanosheets was considered to be associated with the intrinsic growth of MoO_3 nuclei owing to the layered crystal structure, along with its reduction by ethanol at elevated solvothermal temperatures (Supporting Information, Scheme S1).

Figure 2 a shows the UV/Vis–NIR spectra of the MoO_{3-x} products and commercial MoO_3. As can be seen, a strong absorption peak located at approximately 680 nm associated with LSPR is clearly observed in the spectra of MoO_{3-x} nanosheets. It is worth noting that such a strong LSPR peak in the visible range is seldom found in the plasmonic semiconductor nanostructures, which usually appear in the NIR–mid infrared (MIR) region.[13] In contrast, commercial MoO_3 samples exhibit only a UV-light response, with the absorption edge at about 400 nm, which corresponds to its wide band gap (ca. 3.1 eV).

The experimental parameters (e.g., solvothermal temperatures, H_2O_2 volumes, and solvents) played great roles in determining the phase structures and plasmonic resonances of the products (Table S1). When the reaction temperature was lowered from 160 °C to 140 °C, light-blue quasi-uniform molybdenum oxide nanosheets with smaller sizes were obtained (Figure S1). As seen from the UV/Vis–NIR diffuse reflectance spectra (Figure 2 A), the corresponding LSPR wavelength was red shifted to about 950 nm, along with decreased absorption peak intensity. Upon raising the reaction temperature to 180 °C, the product was changed into monoclinic MoO_2 (Figure S1). In the synthesis of MoO_{3-x} nanostructures, ethanol not only performs as the solvent, but is employed as the reducing agent. In fact, ethanol was partially oxidized to aldehyde during solvothermal treatments, which was verified by chemical analysis (silver mirror test) of the resulting supernatant liquor. Upon increasing the temperature from 140 to 160 °C, the stronger reducibility of ethanol enables MoO_3 to generate more oxygen vacancies, thereby leading to deficient MoO_{3-x} with sufficient free carriers to support LSPR. However, too high of a temperature (180 °C) caused the phase transformation from orthorhombic MoO_3 into the metallic monoclinic MoO_2.

The choice of solvents was also a key factor in tailoring the plasmonic wavelength of MoO_{3-x}. Instead of ethanol, other kinds of alcohols, such as 1-butanol and 2-propanol, could also produce blue products, in which larger nanosheets of molybdenum oxide products were found (Figure S2). With a red shift in the LSPR wavelengths, the absorption bands were observed at around 870 and 950 nm for products resulting from the use of 1-butanol and 2-propanoal as the solvents, respectively (Figure 2 b). This is attributed to the difference in the reducibility of the alcohols, which follows the order of ethanol > 1-butanol > 2-propanol. To verify the role of alcohol, a control experiment was implemented using a non-reductive solvent (acetonitrile) while keeping the other conditions unchanged. However, only hexagonal MoO_3 microrods with no LSPR absorption (Figure S3) were produced.

To elucidate the oxidation state of Mo in the plasmonic MoO_{3-x} nanostructures, X-ray photoelectron spectroscopy (XPS) measurements were carried out. Figure 3 a displays the Mo 3d XPS core spectra of the as-prepared MoO_{3-x} and commercial MoO_3. As can be seen, only Mo^{6+} exists in the commercial MoO_3, whereas both Mo^{6+} and Mo^{5+} are present in the MoO_{3-x} nanosheets. For the commercial MoO_3 sample, two peaks (232.6 and 235.7 eV) are attributed to the $3d_{5/2}$ and $3d_{3/2}$ of Mo^{6+}, respectively.[14] In contrast, the peaks of Mo $3d_{5/2}$ and $3d_{3/2}$ shift to lower binding energies, and both of them can

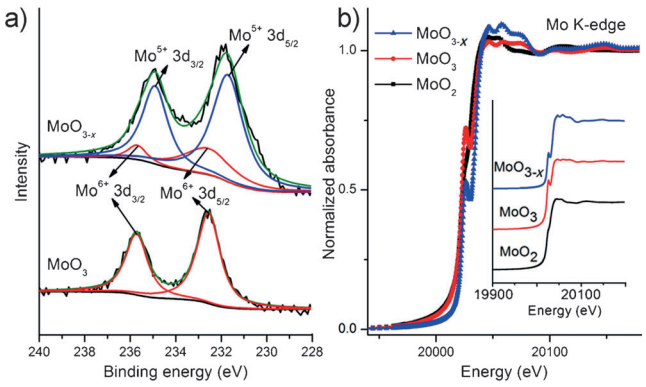

Figure 3. a) Mo 3d XPS spectra of the as-prepared MoO_{3-x} and commercial MoO_3 samples. b) Mo K-edge XANES spectra of MoO_{3-x} and reference materials (commercial MoO_3 and MoO_2).

be divided into two separate peaks. The peaks at 232.6 and 235.7 eV correspond to Mo^{6+}, and those centered at 231.7 and 234.9 eV are assigned to Mo^{5+}.[14] According to the XPS peak area of Mo 3d, the Mo^{6+} and Mo^{5+} cations account for 22.7% and 77.3% of the total Mo states, respectively, in the MoO_{3-x} nanosheets. The average oxidation state of Mo is thus determined to be 5.23, which is manifestly the mixed-valence state arising from the oxygen vacancies. Furthermore, X-ray absorption fine structure (XAFS) measurements were also conducted to obtain the structural information.[15] Figure 3b shows the normalized X-ray absorption near-edge structure (XANES) spectra at the Mo K-edge for MoO_3, MoO_2, and the prepared MoO_{3-x}. Owing to the 1s→4d electronic transition for tetragonal symmetry, the XANES spectrum of MoO_3 displays a strong pre-edge peak.[16] This feature is also observed in the spectrum of the MoO_{3-x} sample. Yet, it is not observed in MoO_2, which is coordinated by regular octahedrons. Additionally, through the use of an energy shift above the K-edge position, the average valence state of Mo can be identified from the linear fit to the reference samples (Mo foil, MoO_2, and MoO_3).[17] On the basis of this linear fit (Figure S4), the oxidation state of Mo in the MoO_{3-x} nanosheets is calculated to be 5.28, which is in good agreement with the XPS results. From the Fourier transform (FT) k^3-weighed extended X-ray absorption fine structure (EXAFS, Figure S5), it is also seen that MoO_{3-x} is located between MoO_3 and MoO_2.

One crucial application of the plasmonic nanostructures is catalysis. As is known, ammonia borane (NH_3BH_3) contains as high as 19.6 wt% of hydrogen, and exceeds that of gasoline, which makes it an attractive candidate for next-generation chemical hydrogen storage materials.[18] In the presence of a suitable catalyst, the hydrolysis of NH_3BH_3 would take place and H_2 could thus obtained at ambient conditions, as illustrated in Equation (1).

$$NH_3BH_3 + 2\,H_2O \xrightarrow{\text{catalyst}} NH_4^+ + BO_2^- + 3\,H_2 \qquad (1)$$

Recently, a variety of noble metal nanostructures, such as Ru, Rh, and Pt, have been reported to show high activity for H_2 generation from NH_3BH_3 solutions.[19] Given the practical applications, it is essential to develop earth-abundant catalysts with low cost and high efficiency. In this work, the absence of surfactants in the synthetic procedure endows plasmonic MoO_{3-x} with the feasibility and simplicity to investigate their catalytic performance for NH_3BH_3 dehydrogenation, avoiding the additional surface treatments.

Figure 4 displays the time course of H_2 production from NH_3BH_3 aqueous solution at room temperature, both in the dark and under visible light irradiation ($\lambda > 420$ nm). Without

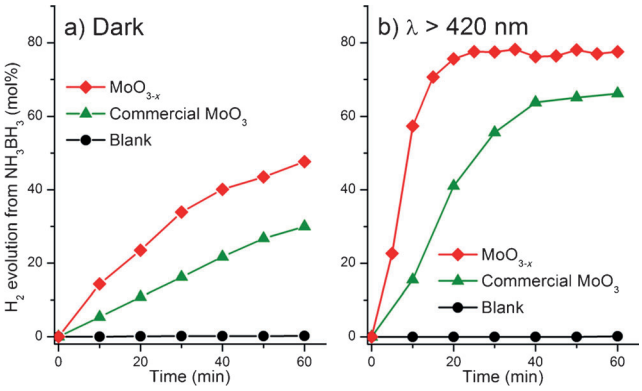

Figure 4. Time course of H_2 evolution from NH_3BH_3 aqueous solution at room temperature for different samples: a) in the dark and b) under visible light irradiation ($\lambda > 420$ nm).

catalysts, NH_3BH_3 was quite stable in water and no H_2 was monitored by gas chromatography, even when exposed to visible light irradiation. We first measured their catalytic performance in the dark. H_2 was easily obtained in the presence of MoO_{3-x} nanosheets and commercial MoO_3 samples, which increased with approximate linearization (Figure 4a). After reaction for 60 min in the dark, about 47.6 mol% of H_2 was generated over the MoO_{3-x} sample, whose initial reaction rate (1.43 mol% min^{-1}) was faster than that of commercial MoO_3 (0.54 mol% min^{-1}). Intriguingly, H_2 evolution was dramatically enhanced when the reaction was carried out under visible light irradiation (Figure 4b). The MoO_{3-x} nanosheets could produce 57.4 mol% of H_2 in the initial 10 min, and almost reached the maximum (75.6 mol%) within 20 min. In contrast, commercial MoO_3 could yield 15.5 mol% of H_2 in the initial 10 min, and it took about 40 min to reach its maximum (63.8 mol%). The initial H_2 yield rate over MoO_{3-x} nanosheets (5.74 mol% min^{-1}) was 3.7 times faster than that of commercial MoO_3 (1.55 mol% min^{-1}). Under visible-light irradiation, the plasmonic MoO_{3-x} displayed a two-fold higher initial H_2 yield rate than the Ag/SBA-15 samples with the best activity (ca. 2.67 mol% min^{-1})[20] under the same conditions (Figure S6). In contrast to experiments conducted in the dark, H_2 production was enhanced approximately four-fold under visible light irradiation over the plasmonic MoO_{3-x} nanosheets. To the best of our knowledge, this is the first report concerning visible-light-induced hydrogen evolution enhancement from NH_3BH_3 solution in plasmonic semiconductor materials.

To eliminate the possible effect of band-gap excitation on the catalytic activity of MoO_{3-x}, visible-light irradiation with a longer wavelength ($\lambda > 450$ nm) was also carried out (Figure S7). Similar activity was found for MoO_{3-x}, thus confirming the lack of a contribution from band-gap excitation. Apart from visible light, light irradiation from a Xe lamp with $\lambda > 420$ nm still contains some infrared light. Owing to the wide infrared-light absorption of the plasmonic MoO_{3-x} nanosheets, the temperature of the suspension was found to increase by about 15 °C under light irradiation. To demonstrate the contribution of this photothermal effect, a control experiment at 40 °C was performed with MoO_{3-x} in the dark (Figure S8). The initial H_2 yield rate in the dark at 40 °C was 2.42 mol % min^{-1}, which was a little higher than the production at room temperature (25 °C, 1.43 mol % min^{-1}) and much lower than that under light irradiation (5.74 mol % min^{-1}). Therefore, the H_2 production enhancement upon light irradiation is predominantly due to the plasmonic catalysis of MoO_{3-x} nanosheets, and photothermal heating only accounts for a small portion (about 23 %).

By using monochromatic light ($\lambda = 440$ nm or 480 nm) and a red LED lamp with $\lambda_{max} = 650$ nm, the wavelength-dependence for H_2 production enhancement was also investigated (Figure S9). The reaction rate increase for H_2 production was in line with the light absorption of the MoO_{3-x} nanosheets, suggesting that the enhancement of the activity can be attributed to the LSPR effect of MoO_{3-x} nanosheeets.[2,20] The maximum performance was found by using red LED light irradiation, whose initial H_2 production rate (2.50 mol % min^{-1}) was 1.8 times that in the dark condition.

The significant enhancement of H_2 production under light irradiation is regarded to be related to the strong light-harvesting of MoO_{3-x} nanosheets induced by LSPR. To validate this, $NaHCO_3$ (as a positive charge scavenger) was introduced into the suspension of MoO_{3-x} samples in the dark and under visible light irradiation conditions for NH_3BH_3 dehydrogenation. In both cases, H_2 production was greatly decreased (Figure S10). Moreover, the inhibition of catalytic performance in the presence of $NaHCO_3$ under visible light irradiation was higher than in the dark. As can be derived from the strong LSPR, MoO_{3-x} could be excited by visible light and generate electron–hole pairs. As HCO_3^- is highly adsorbed on the surface of catalysts, and can react with a positive charge,[21] the activation of NH_3BH_3 is strikingly restrained. While for the commercial MoO_3 sample, it was partially reduced by NH_3BH_3 and its color was changed to blue after the reaction (Figure S11), thus making it responsive to visible light. Therefore, a similar enhancement effect of H_2 production under visible light irradiation was also observed for commercial MoO_3 sample. The catalytic stability of the plasmonic MoO_{3-x} sample was measured by recovering it, and after three repeated cycles it still showed considerable activity (Figure S12). In addition, the structural and optical stability of the MoO_{3-x} sample was further confirmed by XRD patterns and UV/Vis–NIR diffuse reflectance spectra (Figures S13 and S14) before and after the recycling tests, which reveals the potential application of the plasmonic semiconductor nanostructures as efficient and stable catalysts.

In summary, well-defined 2D MoO_{3-x} nanosheets were obtained by a nonaqueous approach. The prepared MoO_{3-x} nanosheets display strong LSPR in the visible region, which can be tuned by varying the experimental parameters. Under visible light irradiation, such plasmonic MoO_{3-x} nanosheets showed dramatically enhanced H_2 evolution from NH_3BH_3 solutions by over a factor of four compared to that performed in the dark. This work illustrates a rational route to plasmonic MoO_{3-x} nanosheets, which may offer a generalized method for generating other semiconductor nanostructures with LSPR, such as deficient vanadium and tungsten oxides. The absence of surfactants permits further investigation in the fields of in vivo bioimaging, gas sensors, photothermal cell therapy, and so on.

Received: November 9, 2013
Revised: December 14, 2013
Published online: February 12, 2014

Keywords: heterogeneous catalysis · hydrogen generation · molybdenum oxide · nanostructures · surface plasmon resonance

[1] J. A. Fan, C. Wu, K. Bao, J. Bao, R. Bardhan, N. J. Halas, V. N. Manoharan, P. Nordlander, G. Shvets, F. Capasso, *Science* **2010**, *328*, 1135.
[2] S. Linic, P. Christopher, D. B. Ingram, *Nat. Mater.* **2011**, *10*, 911.
[3] W. A. Murray, W. L. Barnes, *Adv. Mater.* **2007**, *19*, 3771.
[4] a) M. Rycenga, C. M. Cobley, J. Zeng, W. Y. Li, C. H. Moran, Q. Zhang, D. Qin, Y. N. Xia, *Chem. Rev.* **2011**, *111*, 3669; b) H. J. Chen, L. Shao, Q. Li, J. F. Wang, *Chem. Soc. Rev.* **2013**, *42*, 2679; c) K. Mori, M. Kawashima, M. Che, H. Yamashita, *Angew. Chem.* **2010**, *122*, 8780; *Angew. Chem. Int. Ed.* **2010**, *49*, 8598; d) H. Cheng, B. Huang, P. Wang, Z. Wang, Z. Lou, J. Wang, X. Qin, X. Zhang, Y. Dai, *Chem. Commun.* **2011**, *47*, 7054; e) A. Tanaka, K. Hashimoto, H. Kominami, *J. Am. Chem. Soc.* **2012**, *134*, 14526.
[5] K. L. Kelly, E. Coronado, L. L. Zhao, G. C. Schatz, *J. Phys. Chem. B* **2003**, *107*, 668.
[6] A. Boltasseva, H. A. Atwater, *Science* **2011**, *331*, 290.
[7] M. Kanehara, H. Koike, T. Yoshinaga, T. Teranishi, *J. Am. Chem. Soc.* **2009**, *131*, 17736.
[8] a) J. M. Luther, P. K. Jain, T. Ewers, A. P. Alivisatos, *Nat. Mater.* **2011**, *10*, 361; b) Y. X. Zhao, H. C. Pan, Y. B. Lou, X. F. Qiu, J. J. Zhu, C. Burda, *J. Am. Chem. Soc.* **2009**, *131*, 4253; c) S. W. Hsu, K. On, A. R. Tao, *J. Am. Chem. Soc.* **2011**, *133*, 19072.
[9] R. Buonsanti, A. Llordes, S. Aloni, B. A. Helms, D. J. Milliron, *Nano Lett.* **2011**, *11*, 4706.
[10] K. Manthiram, A. P. Alivisatos, *J. Am. Chem. Soc.* **2012**, *134*, 3995.
[11] T. R. Gordon, M. Cargnello, T. Paik, F. Mangolini, R. T. Weber, P. Fornasiero, C. B. Murray, *J. Am. Chem. Soc.* **2012**, *134*, 6751.
[12] Q. Huang, S. Hu, J. Zhuang, X. Wang, *Chem. Eur. J.* **2012**, *18*, 15283.
[13] a) Y. X. Zhao, C. Burda, *Energy Environ. Sci.* **2012**, *5*, 5564; b) G. V. Naik, V. M. Shalaev, A. Boltasseva, *Adv. Mater.* **2013**, *25*, 3264.
[14] M. Vasilopoulou, A. M. Douvas, D. G. Georgiadou, L. C. Palilis, S. Kennou, L. Sygellou, A. Soultati, I. Kostis, G. Papadimitropoulos, D. Davazoglou, P. Argitis, *J. Am. Chem. Soc.* **2012**, *134*, 16178.
[15] Y. Kuwahara, K. Nishizawa, T. Nakajima, T. Kamegawa, K. Mori, H. Yamashita, *J. Am. Chem. Soc.* **2011**, *133*, 12462.

[16] T. Ressler, R. E. Jentoft, J. Wienold, M. M. Günter, O. Timpe, *J. Phys. Chem. B* **2000**, *104*, 6360.
[17] a) V. T. T. Ho, C. J. Pan, J. Rick, W. N. Su, B. J. Hwang, *J. Am. Chem. Soc.* **2011**, *133*, 11716; b) T. Ressler, J. Wienold, R. E. Jentoft, T. Neisius, *J. Catal.* **2002**, *210*, 67.
[18] a) A. Staubitz, A. P. M. Robertson, I. Manners, *Chem. Rev.* **2010**, *110*, 4079; b) A. D. Sutton, A. K. Burrell, D. A. Dixon, E. B. Garner III, J. C. Gordon, T. Nakagawa, K. C. Ott, J. P. Robinson, M. Vasiliu, *Science* **2011**, *331*, 1426.
[19] a) J. M. Yan, X. B. Zhang, T. Akita, M. Haruta, Q. Xu, *J. Am. Chem. Soc.* **2010**, *132*, 5326; b) M. Yadav, Q. Xu, *Energy Environ. Sci.* **2012**, *5*, 9698; c) M. Chandra, Q. Xu, *J. Power Sources* **2007**, *168*, 135.
[20] K. Fuku, R. Hayashi, S. Takakura, T. Kamegawa, K. Mori, H. Yamashita, *Angew. Chem.* **2013**, *125*, 7594; *Angew. Chem. Int. Ed.* **2013**, *52*, 7446.
[21] C. Hu, T. Peng, X. Hu, Y. Nie, X. Zhou, J. Qu, H. He, *J. Am. Chem. Soc.* **2010**, *132*, 857.

